Journal of Physics: Condensed Matter

PAPER

Perpendicular and in-plane hole asymmetry in a strained $NiFe_2O_4$ film

To cite this article: R Knut *et al* 2021 *J. Phys.: Condens. Matter* **33** 225801

IOP Publishing Journal of Physics: Condensed Matter
J. Phys.: Condens. Matter **33** (2021) 225801 (7pp) https://doi.org/10.1088/1361-648X/abf0c5

Perpendicular and in-plane hole asymmetry in a strained $NiFe_2O_4$ film

R Knut[1], R S Malik[1], C Kons[2], J E Shoup[2], F Radu[3], C Luo[3,4], Y O Kvashnin[1], A Gupta[5], O Karis[1] and D A Arena[2,*]

[1] Department of Physics and Astronomy, Uppsala University, Box 516, SE-751 20, Uppsala, Sweden
[2] Department of Physics, University of South Florida, Tampa, FL 33620, United States of America
[3] Helmholtz-Zentrum Berlin für Materialien und Energie, Albert-Einstein-Straße 15, 12489, Berlin, Germany
[4] Institute of Experimental Physics of Functional Spin Systems, Technical University of Munich, James-Franck-Strasse 1, 85748 Garching b. München, Germany
[5] Department of Chemistry and Biochemistry, The University of Alabama, Tuscaloosa, AL 35487, United States of America

E-mail: darena@usf.edu

Received 13 October 2020, revised 2 March 2021
Accepted for publication 22 March 2021
Published 4 May 2021

Abstract

Strained materials can exhibit drastically modified physical properties in comparison to their fully relaxed analogues. We report on the x-ray absorption spectra (XAS) and magnetic circular dichroism (XMCD) of a strained $NiFe_2O_4$ inverse spinel film grown on a symmetry matched single crystal $MgGa_2O_4$ substrate. The Ni XAS spectra exhibit a sizable difference in the white line intensity for measurements with the x-ray electric field parallel to the film plane (normal incidence) vs when the electric field is at an angle (off-normal). A considerable difference is also observed in the Fe $L_{2,3}$ XMCD spectrum. Modeling of the XAS and XMCD spectra indicate that the modified energy ordering of the cation 3*d* states in the strained film leads to a preferential filling of 3*d* states with out-of-plane character. In addition, the results point to the utility of x-ray spectroscopy in identifying orbital populations even with elliptically polarized x-rays.

Keywords: x-ray absorption spectroscopy, x-ray magnetic circular dichroism, ferrimagnets, spinels, thin films, magnetic order, magnetic insulators

(Some figures may appear in colour only in the online journal)

1. Introduction

Coherent strain is one of the principle ways to alter the energy landscape of epitaxial thin films thereby stabilizing ground states and physical properties not found in bulk counterparts [1]. Among other effects, strained thin films can exhibit improved electron mobility [2], metal to insulator transitions [3], suppression or enhancement of superconductivity [4], stabilization of ferroelectricity [5], optical band gap tuning [6–8], modification of long range spin order and anisotropy [9]. Strain in films can also lead to enhanced ionic conductivity [10] and altered vacancy formation [11] and the modified electronic states at the surfaces of strained films can affect catalytic [12, 13] and other chemical properties. Such strain-modulated effects can occur in elemental solids, compound covalent semiconductors, and highly ionic materials such as oxides.

The spinel structure is among the most common types of crystalline materials and can accommodate a wide range of chemical compositions. As a result of this chemical adaptability, the spinel structure can be found in materials with a broad distribution of properties and uses, including highly insulating phases [14, 15], semiconductors [16, 17], metal to insulator transitions [18, 19], transparent conductors [20], and even superconductivity [21, 22]. Magnetically, spinels can span all

* Author to whom any correspondence should be addressed.

forms of magnetic order (paramagnetic, ferromagnetic, antiferromagnetic, and ferrimagnetic, etc) and can exhibit complex behavior including half-metallicity [23–25], spin frustration [26], spin glass formation [27], and support quantum critical points [28, 29]. Strain in thin spinel films can alter the magnetic ground state, leading to effects such as a significant increase of saturation magnetization [30] and enhanced uniaxial magnetic anisotropy [31, 32]. Strain is also an efficient method to alter magneto-elastic coupling [33] and dramatically decrease damping of spin dynamics [34]. In this report, we present *L*-edge x-ray spectroscopy of a strained $NiFe_2O_4$ (NFO) film, indicating that tensile strain in Ni-ferrite films modifies the unit cell symmetry which in turn lifts the degeneracy of the Ni and Fe 3*d*-states. The altered energy landscape results in a very large polarization of the unoccupied Ni 3*d* orbitals.

Spinels have the general chemical formula PQ_2X_4 [35–38] where X is typically a divalent anionic (X^{2-}) chalcogen, such as oxygen or sulphur while P/Q are divalent/trivalent metal cations. The cubic spinel structure is relatively open with a large unit cell containing 56 atoms. In spinel oxides, 32 oxygen anions form a fcc sublattice and leave a network of interstitial sites that are either octahedrally or tetrahedrally coordinated to the oxygen ions. For a normal spinel, eight divalent P^{2+} cations are located on one eighth of the available lattice sites with a local tetrahedral symmetry (T_d, or A sites) and the 16 trivalent Q^{3+} cations occupy one half of available the octahedral sites (O_h, B sites). The net spin order in spinels is governed by the dominant anti-ferromagnetic exchange between the A and B sites [39].

NFO is an inverse spinel, where the divalent Ni^{2+} cations shift to the O_h sub-lattice and one half of the total Fe^{3+} cations move to T_d sites. Hence the NFO structure can be expressed as $(Fe^{3+})[Ni^{2+}Fe^{3+}]O_4$ where the parentheses indicate T_d sites and square brackets denote the O_h sublattice. The net moment in NFO is derived primarily from the Ni^{2+}–O_h cations as the anti-ferromagnetic A–B exchange interaction results in a near-complete compensation of the Fe^{3+} magnetic moments. NFO can be synthesized in the bulk as a fully inverse spinel with a cubic lattice parameter of $a = 0.8345$ nm [34].

2. Experimental

NFO films are grown on [001] oriented spinel $MgGa_2O_4$ (MGO) substrates using pulsed laser deposition in an oxygen-rich environment with a background pressure of 10 mTorr. Additional details on film growth and structural characterization can be found in [34]. The film used in this study is 40 nm thick with lattice parameters of 0.828 nm in-plane (matching the lattice of the MGO substrate) and 0.838 nm out-of-plane, resulting in a compressive in-plane strain of 0.78% and an out-of-plane lattice expansion of 0.42%; these lattice parameters match up well with previous high-resolution *x*-ray diffraction data on similar NFO flims on MGO (cf. Fig. 1 in reference [34]).

X-ray absorption spectra (XAS) and magnetic circular dichroism (XMCD) spectra were collected at the PM2-VEKMAG beam line at the BESSY II synchrotron of the Helmholtz Zentrum Berlin. The beam line endstation is equipped with a superconducting vector magnet capable of supplying a magnetic field of $\mu_0 H = \pm 9$ T along the x-ray beam direction, $\mu_0 H = \pm 2$ T along the orthogonal horizontal axis and $\mu_0 H = \pm 1$ T in all directions [40]. These fields are sufficient to saturate the NFO magnetization in-plane and also in the out-of-plane direction when the film is oriented with the sample normal parallel to the x-ray beam direction [normal incidence (NI)]. The bending magnet x-ray source of PM-2 supplies elliptically polarized x-rays with user-selectable polarization (right- or left-circular or horizontal linear). In these measurements, the degree of circular polarization (CP) was fixed to 77% (RCP) and the XMCD spectra were generated by recording two spectra with saturating magnetic fields applied along two opposite directions ($\pm\mu_0\vec{H}$). XMCD spectra presented below have been corrected for degree of CP and also for angle of incidence. The XAS spectra presented are the average of the two spectra collected with $\pm\mu_0\vec{H}$.

The sample was mounted with the film [100] direction parallel to the horizontal direction ($\hat{x}$ in the laboratory frame). The sample could be rotated about the film [010] axis ($\hat{y}$ in the lab frame). At NI, the electric field from the x-ray beam has both E_x and E_y components (refer to figure 1(b)), i.e. parallel to the [100] and [010] film axes, respectively. When the sample is rotated about the film [010] axis, the E_y component is unchanged, but x-ray projection onto the film now produces $E_{x'}$ and $E_{z'}$ components with $E_{x'}$ still parallel to the NFO [100] axis and $E_{z'}$ oriented parallel to the NFO [001] axis. For the off-normal incidence (O-NI) measurements, θ is fixed to 45° and hence $|E_{x'}| = |E_{z'}| = |E_x|/\sqrt{2}$.

A photodiode was mounted behind the sample to collect XAS and XMCD spectra in luminescence yield (LY) mode. In LY, x-rays pass through the film and onto the substrate where they can excite photon energy down conversion into the UV/visible range via x-ray emitted optical luminescence (XEOL) [41]. The XEOL spectrum from the substrate alone is relatively energy-independent at x-ray energies away from absorption edges and the XEOL signal is recorded by the photodiode as the x-ray energy is swept through the Fe and Ni $L_{2,3}$ core levels. Strong resonant x-ray absorption in the NFO films at these energies reduces the flux of x-rays reaching the substrate, thereby turning the substrate into a detector of the transmission x-ray spectrum of the NFO film. XAS are generated from the transmission signal via Beer's law.

3. XAS and XMCD spectroscopy

Figures 2(a) and 3(a) present the magnetization averaged (sum of individual spectra collected with $\pm\mu_0\vec{H}$) XAS spectra of Ni and Fe from the NFO film. For both the Ni and Fe spectra, a small linear pre-edge contribution has been subtracted and the post-edge intensity ($h\nu \sim 875$ eV for Ni and $h\nu \sim 735$ eV for Fe) has been set to unity. The resulting XAS spectra are therefore proportional to the x-ray absorption per Ni or Fe atom. The XMCD spectra for Ni or Fe are generated from the difference of the two $\pm\mu_0\vec{H}$ XAS spectra, correcting for the degree

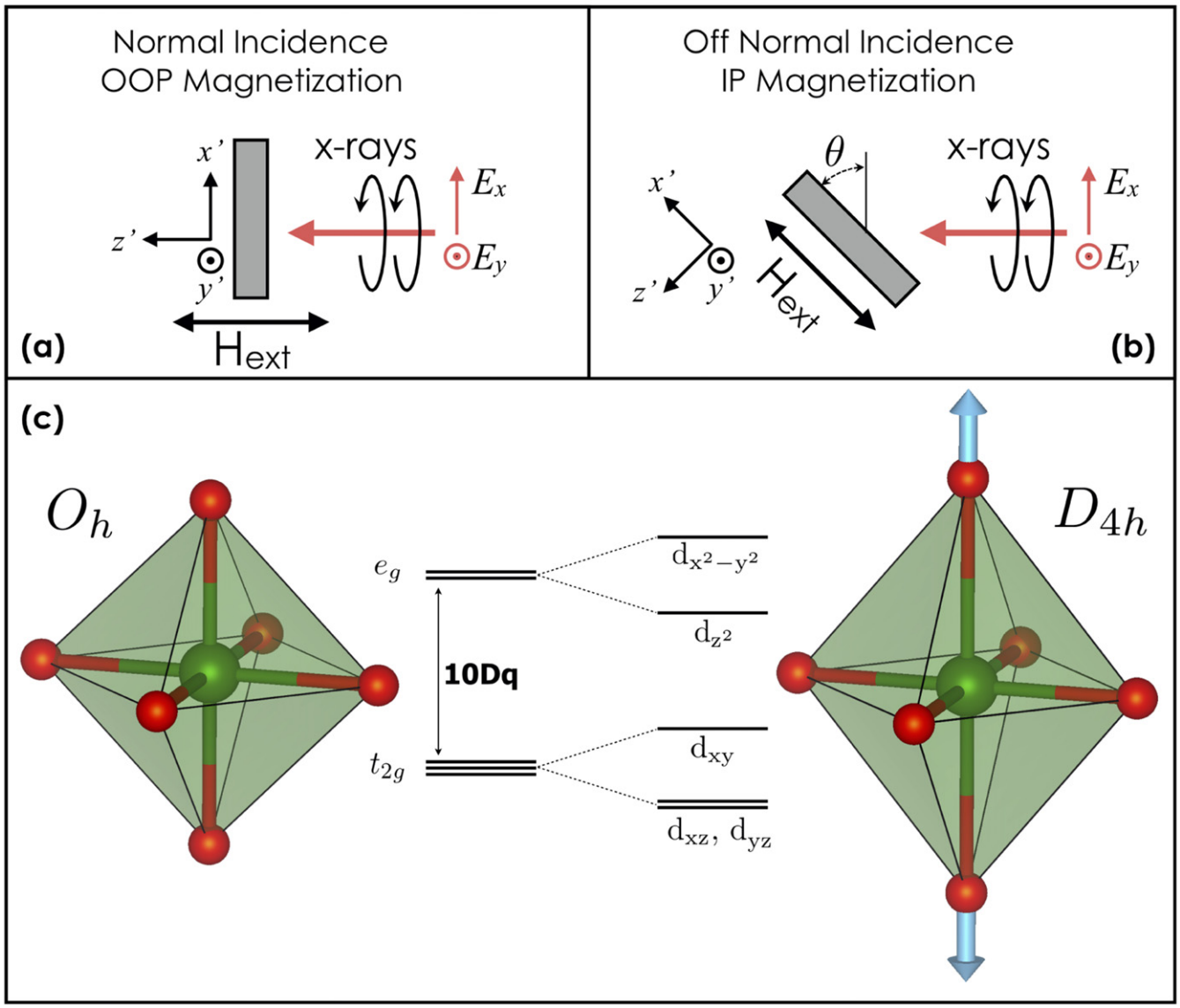

Figure 1. (a) and (b) Experimental geometry. In (a) the elliptically polarized x-rays impinge the NFO sample (grey rectangle) at NI, with electric field vectors E_x and E_y parallel to the sample [100] (x') and [010] (y') directions. In this geometry the external magnetic field (H_{ext}) was applied perpendicular to the sample surface. In (b) the sample is rotated by 45°. E_y remains parallel to the sample [010] direction but E_x now has components parallel to [100] and [001] (z'); H_{ext} is parallel to the film plane. (c) Effect of tetragonal distortion on the $Ni^{2+}3d$ orbitals. Elongation of the O_h bi-pyramid (blue arrows) lifts the degeneracy of the e_g states, leading to preferential filling of the d_{z^2} orbital and consequently leaving additional holes in the $d_{x^2-y^2}$ orbital.

of CP (77%) and also the angle of incidence (45°) in the case of the O-NI Fe and Ni spectra.

We begin by discussing the Ni XAS spectra in figure 2(a). The XAS spectrum collected at NI is presented as a solid grey line while the spectrum collected at O-NI is depicted as a solid magenta line. The shapes of the two Ni spectra are similar and the XAS spectra divide into two prominent and spin–orbit split features with absorption from the L_3 edge ($2p_{3/2}$ level) between ~850–857 eV and the L_2 edge ($2p_{1/2}$ level) spanning x-ray energies of ~867–872 eV. The L_2 portion of the spectra exhibits two primary peaks labeled A and B in the figure. Overall, the shapes of the Ni XAS spectra are consistent with previously published reports [42–44] and indicate that the Ni cations are in a 2^+ oxidation state in an apparent octahedral crystal field environment. The large variation in the intensity of the Ni $2p$ XAS spectra between the NI and O-NI spectra is discussed below.

Turning to the magnetism of the Ni cations, the XMCD spectra are presented in figures 2(b) (NI) and (c) (O-NI). For the NI spectra, an external magnetic field of $\mu_0 H = \pm 2$ T was used to saturate the magnetization perpendicular to the film plane. For the O-NI measurements, and in-plane field of $\mu_0 H = \pm 1$ T was sufficient to saturate the magnetization in-plane. The Ni XMCD intensity for both sample orientations has been normalized to unity at the dominant negative XMCD peak at 852.5 eV; the un-normalized XMCD spectra also display a similar variation in peak intensity as the XAS scans in figure 2(a). As with the XAS, the two Ni XMCD

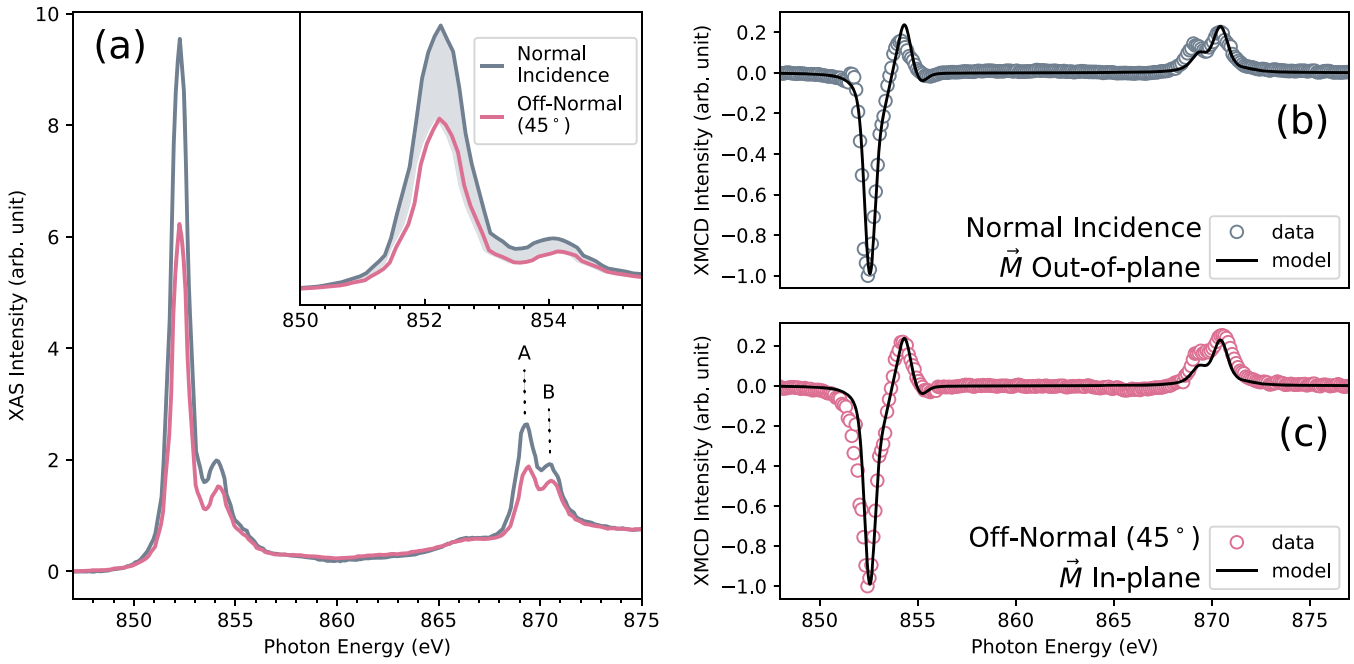

Figure 2. (a) Polarization-averaged XAS scans of the Ni $L_{2,3}$ edges from a strained NFO film on MGO. The pre-edge contribution has been subtracted and the post-edge normalized to unity. Large intensity asymmetries are evident, as highlighted in the inset to the figure. (b) Grey markers: normalized XMCD spectrum for Ni in the NI configuration ($\vec{H} \parallel z'$). Black line: calculated XMCD spectrum for Ni^{2+}. See text for calculation details. (c) Same as in (b) but for the O-NI ($\theta = 45°$, $\vec{H} \| x'$) configuration.

spectra exhibit nearly the same line shape. The L_3 portion of the XMCD spectra is characterized by a prominent negative peak at 852.5 eV and a positive shoulder about 2 eV higher followed by a flat response until the positive peaks of the L_2 edge between 868–872 eV. The XMCD scans for both NI and O-NI orientations are again consistent with the spectra expected from Ni^{2+} in an octahedral crystal field.

Figure 3(a) presents the Fe $L_{2,3}$ magnetization averaged XAS spectra and XMCD scans are shown in figures 3(b) (NI) and (c) (O-NI); the XMCD spectra are measured in the same field conditions as the Ni XMCD presented in figures 2(b) and (c). As with the Ni XAS spectra, the shape of the Fe absorption is quite similar. Unlike the Ni scans, there is little variation in intensity between the two sample angles. The Fe XAS spectra indicate the dominant Fe valence is 3^+ [43], as expected for NFO. A contribution from Fe^{2+}, which can be observed in oxygen deficient films, could not be resolved. The dichroism spectra in figures 3(b) and (c) are also normalized to unity at the dominant negative peak located at 709.5 eV. For both the NI and O-NI configurations the L_3 XMCD spectrum exhibits a distinctive negative/positive/negative structure (labeled A, B, C in the figure) common to many Fe containing spinels [42, 43, 45–52]. Unlike the Ni XMCD spectrum, however, there is a considerable variation in the Fe XMCD line shape between the NI and O-NI configurations. For the NI spectra (out-of-plane magnetization), feature A is clearly less intense than feature C while in the O-NI orientation (in-plane magnetization), the two features have nearly equal intensity. The origin of this asymmetry between the out-of-plane and in-plane magnetization directions, as well as the large variation in the Ni XAS intensity, is discussed in the following section.

4. Discussion

The most striking aspect of the Ni XAS is the large intensity difference between the NI and O-NI spectra as seen in the inset to figure 2(a), which is reminiscent of the asymmetric hole distribution in the Cu d-holes of high T_c superconductors and related compounds [53]. The XAS spectra have been normalized to the absorption proportional per Ni atom, hence the XAS intensity reveals a substantial variation in the number of final states available for the dipole allowed x-ray absorption process. Restricting our discussion to the Ni L_3 edge, we find normalized intensity difference, $R_{\Delta I} = (I_{\mathrm{NI}} - I_{\mathrm{O-NI}})/I_{\mathrm{NI}}$, is $\simeq$30%, indicating that there is a large angular dependent variation in the dipole-allowed $2p_{3/2} \rightarrow 3d$ transition. Here, I_{NI} and $I_{\mathrm{O-NI}}$ denote the Ni L_3 intensity in the NI and O-NI geometries, respectively. The large $R_{\Delta I}$ is even more remarkable when we consider the x-ray polarization. The XAS intensity is proportional to the number of holes in the Ni $3d$ manifold and the large $R_{\Delta I}$ must originate from an asymmetry between the number of $3d$ holes probed between the NI and O-NI orientations. With elliptically polarized light, there is a common origin to a large fraction of the XAS signal between the NI and O-NI configurations. The contributions from Ni $3d$ holes distributed along the NFO [010] axis (originating from E_y) remains unchanged between the NI and O-NI spectra, and a portion of the XAS signal from holes along the NFO [100] direction (originating from E_x or $E_{x'}$) is also common to both orientations. Hence the

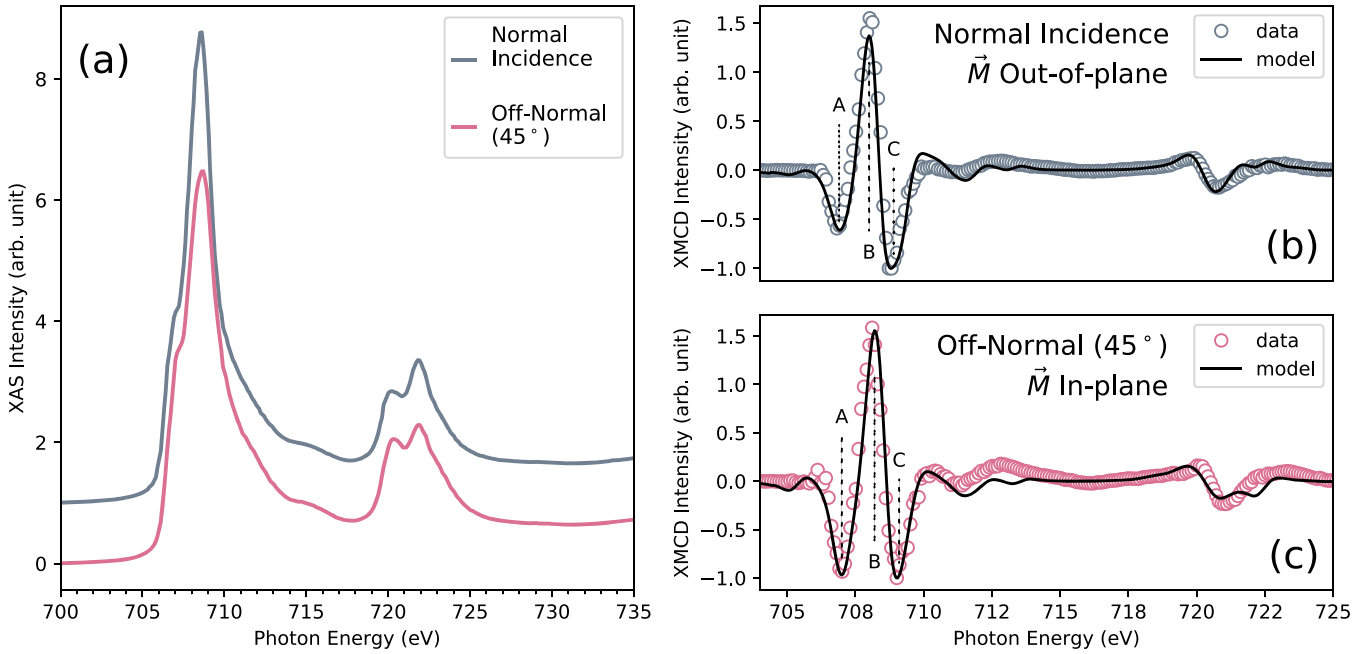

Figure 3. (a) Polarization-averaged XAS scans of the Fe $L_{2,3}$ edges from a strained NFO film on MGO; for clarity, spectra have been offset vertically. The pre-edge contribution has been subtracted and the post-edge normalized to unity. The Fe XAS for the NI and off-normal orientations are quite similar. (b) Fe XMCD spectrum (grey dots) for the NI orientation ($\vec{H}\|z'$). The dip/peak/dip (labeled A, B, C) structure of many Fe spinel compounds is evident. (c) Same as in (b) but in the off-normal configuration with $\vec{H}\|x'$. In (b) and (c) the black line is a calculated spectrum generated from a linear combination of $Fe^{3+}_{O_h}$, $Fe^{3+}_{T_d}$ and $Fe^{2+}_{O_h}$. Refer to text for calculation details.

significant variation in the XAS intensity stems from a very large asymmetry in Ni $3d$ holes that are distributed either in-plane (along [100] and [010]) or out-of-plane (along the NFO [001] direction).

The large difference in the Ni L_3 XAS intensity can be used to estimate the ratio of the Ni holes with in-plane character to the total number of Ni holes. We assume that the number of holes along the [100] and [010] in-plane directions are equal: $n_{100} = n_{010} = n_{\|}$ but the number of holes with out-of-plane character ($n_{\perp}$) may be different. $R_{\Delta I}$ can be related to $n_{\|}$ and $n_{\perp}$ as: $R_{\Delta I} = \sin^2\theta(n_{\|} - n_{\perp})/n_{\|}(1+\alpha^2)$. Here, α is defined on the polarization ellipse as the ratio of the semi-minor axis (E_y) to the semi-major axis (E_x) and α can be related to the degree of CP as: $\mathrm{CP} = 2\alpha/1+\alpha^2$. Further assuming that $n_{\|} = \beta n_{\perp}$, the normalized XAS intensity ratio can be expressed as: $R_{\Delta I} = \sin^2\theta(1-\beta)/(1+\alpha^2)$. In our measurements at the VEKMAG beam line, $\mathrm{CP} = 0.77$, resulting in $\alpha^2 = 0.22$ and thus $\beta \simeq 0.20$. The total number of holes (n_{tot}) is the sum of $n_{100} = n_{\|}$, $n_{010} = n_{\|}$ and $n_{001} = n_{\perp} = \beta n_{\|}$ and hence $n_{\perp}/n_{\mathrm{tot}} = \beta/2 + \beta = 0.09$. This is a significant reduction of $n_{\perp}/n_{\mathrm{tot}} = 1/3$ expected for an isotropic distribution of holes.

Modeling of the Ni XAS provides insight into the large difference in the XAS intensity between the NI and O-NI sample orientations. We used the CTM4XAS program to model our spectra. The program utilizes an atomic multiplet approach to calculate dipole-allowed $2p \rightarrow 3d$ transitions combined with ligand field theory that alters the symmetry and energy levels of the final state $3d$ manifold [54]. For the Ni spectra, the Slater F_{dd} integral was reduced to 80% of atomic values while the F_{pd} and G_{gd} integrals were reduced to 90%. Lifetime and instrumental broadening effects were included by convolving the line spectra with Lorentzian and Gaussian distributions of 0.2 eV each. However, the intensity ratio of the Ni L_2 spectrum, labeled A and B in figure 2(a), could not be reproduced with realistic values of the crystal field parameter $10Dq$; only with $10Dq > 2.3$ eV could the ratio between A and B be reproduced. By reducing the symmetry of the local crystal field around the Ni^{2+} cation to D_{4h}, applicable to tetragonal systems and square-planar molecules such as XeF_4, the modeling resulted in a much better fit of the Ni spectrum with $10Dq = 1.1$ eV, comparable to many other estimates for Ni in O_h symmetry in NFO and related compounds [43, 44, 46]. This symmetry lowering transition of the NFO lattice under the substrate-induced strain may also explain the large XAS intensity variation between the NI and O-NI sample orientations.

In an O_h crystal field the valence $3d$ manifold splits into the lower energy t_{2g} orbitals (d_{xy}, d_{yz} and d_{xz}) and the higher energy e_g group ($d_{3z^2-r^2}$ and $d_{x^2-y^2}$). Within a group the orbitals are degenerate and the t_{2g} and e_g groups are separated by the crystal field parameter $10Dq$. For Ni^{2+} with a $3d^8$ valence configuration, Hund's rules filling of the orbitals results in a filled t_{2g} manifold and half-filled e_g orbitals, one with in-plane orbital orientation ($d_{x^2-y^2}$) and the other with out-of-plane character ($d_{3z^2-r^2}$). For the magnetization-averaged XAS spectra, the crystal [100], [010], and [001] axes are equivalent and there would be an equal distribution of holes along each direction. Hence there should be little intensity

variation upon rotation of the sample. However the compressive strain on the NFO film from the MGO substrate stretches the Ni—oxygen octahedra along the [001] axis, separating the apical oxygen anions and weakening their contribution to the crystal field. The remaining four oxygen anions are arranged in a square-planar configuration with respect to the central Ni^{2+} cation so that the effective crystal field takes on more of a D_{4h} character. In a D_{4h} point-group symmetry, the three orbitals with out-of-plane character, that is, the d_{yz} and d_{xz} orbitals from the t_{2g} group and the $d_{3z^2-r^2}$ orbital from the e_g group, have their energy lowered with respect to their values under O_h symmetry [55]. The energy splitting is parameterized by an additional crystal field parameter D_s and the intensity ratio of the A and B peaks in the Ni L_2 edge could be modeled with $10Dq = 1.1$ eV and $D_s = 0.47$ eV. The strain-induced compression of the Ni–O bonds along the in-plane [100] and [010] axes and stretching along the out-of-plane [001] axis therefore results in preferential filling of the out-of-plane orbitals, leaving the majority of the unoccupied Ni 3*d* states with an in-plane orbital character. The result decreases the ratio $n_\perp/n_{tot}$, as is strongly suggested by the large difference in I_{NI} and I_{O-NI}.

The XMCD spectra of Ni and Fe were also modeled with the multiplet approach, as can be seen in figures 2(b) and (c) (Ni) and 3(b) and (c) (Fe). The Ni XMCD spectra could be reproduced quite satisfactorily for both sample orientations assuming a Ni^{2+} cation with $10Dq = 1.1$ eV and an exchange field of 10 meV. No further contributions to the Ni XMCD spectra were necessary. The modeling confirms that the XMCD spectra for Ni arise from the contributions of a single Ni cation species.

The XMCD spectra for Fe are more complex. First, the Fe cations occupy both O_h and T_d sub-lattice sites with a strong anti-ferromagnetic interaction between the two lattices. Also, there may be a contribution from Fe^{2+} cations in addition to the dominant Fe^{3+} species and the effect of this small fraction may be more pronounced in the dichroism than in the magnetically averaged XAS. And indeed, we find that a small Fe^{2+} contribution is needed to reproduce the experimental spectra. Model spectra indicate that for both sample orientations, peak A in the dichroism spectrum is derived primarily from Fe^{2+} on the O_h sub-lattice. The spectral contribution from Fe^{3+}–O_h is associated primarily with peak C and the oppositely aligned feature B is derived from tetrahedrally-coordinated Fe^{3+} cations. For the NI Fe spectrum in figure 3(b), where the magnetization is saturated out-of-plane, good agreement with the experimental spectrum can be achieved with a $Fe^{2+}_{O_h}$:$Fe^{3+}_{T_d}$:$Fe^{3+}_{O_h}$ ratio of 0.09:0.46:0.46. This distribution is similar to other reports of NFO [43, 46], which is expected as the ratio of intensities for features A, B and C in the XMCD spectrum is similar to earlier reports. The cation ratios are considerably different for the O-NI (in-plane magnetization) spectrum. For the model spectrum shown in black in figure 3(c), the $Fe^{2+}_{O_h}$:$Fe^{3+}_{T_d}$:$Fe^{3+}_{O_h}$ distributions are 0.26:0.44:0.29. The additional contribution from Fe^{2+}–O_h is necessary to increase the intensity of peak A as seen in the figure.

The differences in the XMCD spectra between the NI and O-NI configurations are consistent with the strong Ni XAS asymmetry seen in figure 2(a). Fe^{3+} has a $3d^5$ valence configuration, generating a half-filled 3*d* manifold with a negligible orbital moment. The Fe^{3+} cation is therefore weakly sensitive to the parent O_h crystal field of NFO or the tetragonally distorted D_{4h} symmetry of our NFO film on MGO. On the other hand, Fe^{2+} has a $3d^6$ valence configuration and the D_{4h} symmetry lowers the energy of the states with out-of-plane orbital character. The larger contribution to the Fe XMCD spectrum from $Fe^{2+}_{O_h}$ for the in-plane magnetization condition suggests there are fewer Fe^{2+} paired spins in the d_{xy} and $d_{x^2-y^2}$ orbitals and consequently a larger degree of spin pairing in the *d*-orbitals with out-of-plane character, reflecting the lower energy of these states in D_{4h} symmetry.

5. Conclusion

We measured the Fe and Ni $L_{2,3}$ XAS and XMCD spectra from an epitaxial, strained NFO film at both NI and O-NI. The Ni XAS spectra confirm that the Ni cations maintain a single 2^+ valence but that the substrate-induced strain alters the local point group symmetry around the Ni from O_h to D_{4h}. The symmetry lowering alters the energy spacing of the Ni 3*d* orbitals, favoring filling of orbitals with predominantly out-of-plane character; the preference for un-occupied states with primarily in-plane character is apparent in the large intensity enhancement of the Ni $L_{2,3}$ XAS at NI. The altering of magnetic states from the D_{4h} symmetry is apparent in the XMCD spectra of Fe, where in-plane magnetization (acquired in the O-NI orientation) favors hole formation in-plane, as revealed by the enhanced contribution of the Fe^{2+} cation to the XMCD spectrum for in-plane magnetization.

Linear dichroism is typically the method utilized to probe such differences in orbital occupation. In addition to providing insight into the specific case of the tetragonally distorted NFO films, our results indicate that valuable information on the relative orbital occupations of metal cation states also can be extracted with circularly or elliptically polarized x-rays.

Acknowledgments

We acknowledge support from the University of South Florida Nexus Initiative (UNI) Award, the Swedish Research Council (VR, contracts 2019-03666, 2017-03799, 2016-04524 and 2013-08316), the Swedish Foundation for Strategic Research, project 'SSF Magnetic materials for green energy technology' under Grant No. EM16-0039, the Knut and Alice Wallenberg foundation, STandUP and eSSENCE, for financial support. The Swedish National Infrastructure for Computing (SNIC) is acknowledged for computational resources. The authors acknowledge the financial support for the VEKMAG project and for the PM2-VEKMAG beamline by the German Federal Ministry for Education and Research (BMBF 05K10PC2, 05K10WR1, 05K10KE1) and by HZB. We thank Steffen Rudorff and Hanjo Ryll for technical support. Work at the University of Alabama is supported by NSF

Grant No. ECCS-1509875. This material is based upon work supported by the National Science Foundation under Grant No. ECCS-1952957.

Data availability statement

The data that support the findings of this study are available upon reasonable request from the authors.

ORCID iDs

Y O Kvashnin https://orcid.org/0000-0002-4238-5733
A Gupta https://orcid.org/0000-0002-1785-7209
D A Arena https://orcid.org/0000-0001-7463-6472

References

[1] Schlom D G, Chen L-Q, Fennie C J, Gopalan V, Muller D A, Pan X, Ramesh R and Uecker R 2014 *MRS Bull.* **39** 118
[2] Chu M, Sun Y, Aghoram U and Thompson S E 2009 *Annu. Rev. Mater. Res.* **39** 203
[3] Ogimoto Y, Nakamura M, Takubo N, Tamaru H, Izumi M and Miyano K 2005 *Phys. Rev.* B **71** 060403
[4] Bozovic I, Logvenov G, Belca I, Narimbetov B and Sveklo I 2002 *Phys. Rev. Lett.* **89** 107001
[5] Ederer C and Spaldin N A 2005 *Phys. Rev. Lett.* **95** 257601
[6] Ni G-X, Yang H-Z, Ji W, Baeck S-J, Toh C-T, Ahn J-H, Pereira V M and Özyilmaz B 2014 *Adv. Mater.* **26** 1081
[7] Pellegrino F M D, Angilella G G N and Pucci R 2010 *Phys. Rev.* B **81** 035411
[8] Çakır D, Sahin H and Peeters F M 2014 *Phys. Rev.* B **90** 205421
[9] Rigato F, Estradé S, Arbiol J, Peiró F, Lüders U, Martí X, Sánchez F and Fontcuberta J 2007 *Mater. Sci. Eng.* B **144** 43
[10] Pennycook T J, Beck M J, Varga K, Varela M, Pennycook S J and Pantelides S T 2010 *Phys. Rev. Lett.* **104** 115901
[11] Aschauer U, Pfenninger R, Selbach S M, Grande T and Spaldin N A 2013 *Phys. Rev.* B **88** 054111
[12] Zhang S, Zhang X, Jiang G, Zhu H, Guo S, Su D, Lu G and Sun S 2014 *J. Am. Chem. Soc.* **136** 7734
[13] Khorshidi A, Violet J, Hashemi J and Peterson A A 2018 *Nat. Catal.* **1** 263
[14] Baltzer P K, Lehmann H W and Robbins M 1965 *Phys. Rev. Lett.* **15** 493
[15] Moyer J A, Kumah D P, Vaz C A F, Arena D A and Henrich V E 2012 *Appl. Phys. Lett.* **101** 021907
[16] Storchak V G, Brewer J H, Russo P L, Stubbs S L, Parfenov O E, Lichti R L and Aminov T G 2010 *J. Phys.: Condens. Matter.* **22** 495601
[17] Kim H J, Song I C, Sim J H, Kim H, Kim D, Ihm Y E and Choo W K 2004 *J. Appl. Phys.* **95** 7387
[18] Song M Y, Lin J G, Samant M G and Parkin S S P 2014 *IEEE Trans. Magn.* **50** 1
[19] Lin J G, Song M Y, Lin J W, Samant M G and Parkin S S P 2013 *IEEE Trans. Magn.* **49** 4311
[20] Omata T, Ueda N, Ueda K and Kawazoe H 1994 *Appl. Phys. Lett.* **64** 1077
[21] Chen C L *et al* 2011 *Supercond. Sci. Technol.* **24** 115007
[22] Jin K *et al* 2015 *Nat. Commun.* **6** 7183
[23] Guan T *et al* 2015 *Phys. Rev. Lett.* **115** 087002
[24] Li P, Xia C, Zheng D, Wang P, Jin C and Bai H 2016 *Phys. Status Solidi RRL* **10** 190
[25] Feng M, Shao B, Cao X-W and Zuo X 2016 *IEEE Trans. Magn.* **52** 1
[26] Zakrzewski A V, Gangopadhyay S, MacDougall G J, Aczel A A, Calder S and Williams T J 2018 *Phys. Rev.* B **97** 214411
[27] Nirmala R *et al* 2017 *J. Phys.: Condens. Matter.* **29** 13LT01
[28] Biffin A, Rüegg C, Embs J, Guidi T, Cheptiakov D, Loidl A, Tsurkan V and Coldea R 2017 *Phys. Rev. Lett.* **118** 067205
[29] Gu C *et al* 2018 *Phys. Rev. Lett.* **120** 147204
[30] Wakiya N, Shinozaki K and Mizutani N 2004 *Appl. Phys. Lett.* **85** 1199
[31] Matsumoto M, Sharmin S, Inoue J-i, Kita E and Yanagihara H 2017 *IEEE Trans. Magn.* **53** 1
[32] Budhani R C *et al* 2018 *Appl. Phys. Lett.* **113** 082404
[33] Gray M *et al* 2018 *Phys. Rev. Appl.* **9** 064039
[34] Singh A V *et al* 2017 *Adv. Mater.* **29** 1701222
[35] Gorter E W 1954 *Philips Res. Rep.* **9** 295
[36] Gorter E W 1954 *Philips Res. Rep.* **9** 321
[37] Gorter E W 1954 *Philips Res. Rep.* **9** 403
[38] Broese van Groenou A, Bongers P F, Stuyts A L, van Groenou A, Bongers P F and Stuyts A L 1969 *Mater. Sci. Eng.* **3** 317
[39] Suzuki Y 2001 *Annu. Rev. Mater. Res.* **31** 265
[40] Noll T and Radu F 2017 *Proc. MEDSI'16, Mechanical Engineering Design of Synchrotron Radiation Equipment and Instrumentation* vol 9 (Geneva, Switzerland: JACoW Publishing) pp 370–3
[41] Vaz C A F, Moutafis C, Buzzi M and Raabe J 2013 *J. Electron Spectrosc. Relat. Phenom.* **189** 1
[42] Wakabayashi Y K *et al* 2018 *Phys. Rev. Mater.* **2** 104416
[43] Klewe C, Meinert M, Boehnke A, Kuepper K, Arenholz E, Gupta A, Schmalhorst J-M, Kuschel T and Reiss G 2014 *J. Appl. Phys.* **115** 123903
[44] van der Laan G, Henderson C M B, Pattrick R A D, Dhesi S S, Schofield P F, Dudzik E and Vaughan D J 1999 *Phys. Rev.* B **59** 4314
[45] Richter M C *et al* 2009 *Eur. Phys. J. Spec. Top.* **169** 175
[46] Hoppe M, Döring S, Gorgoi M, Cramm S and Müller M 2015 *Phys. Rev.* B **91** 054418
[47] Moyer J A, Kumah D P, Vaz C A F, Arena D A and Henrich V E 2013 *J. Magn. Magn. Mater.* **345** 180
[48] Moyer J, Vaz C a, Arena D, Kumah D, Negusse E and Henrich V 2011 *Phys. Rev.* B **84** 054447
[49] Takaobushi J *et al* 2007 *Phys. Rev.* B **76** 205108
[50] Kang J-S *et al* 2008 *Phys. Rev.* B **77** 35121
[51]Štichauer L *et al* 2001 *J. Appl. Phys.* **90** 2511
[52] Pellegrin E *et al* 1999 *Phys. Status Solidi b* **215** 797
[53] Garg K B, Saini N L, Merrien N, Studer F, Durcok S and Tourillon G 1993 *Solid State Commun.* **85** 447
[54] Stavitski E and de Groot F M F 2010 *Micron* **41** 687
[55] Miedema P S, Stepanow S, Gambardella P and de Groot F M F 2009 *J. Phys.: Conf. Ser.* **190** 012143